Relation between nanocluster approximation and Soft-Potential Model, the role of keystone nanocluster in the thermal conductivity. — A plateau characterizes the thermal conductivity k(T) of many amorphous materials at temperatures above 1 K together with a maximum in specific heat Cp, called the Boson peak at the same temperature region [1]. It has been believed for over 50 years that those features are the universal property of glasses. Using the analogy of the keystone species concept of ecology, where one species has a disproportionately large effect on its environment relative to its abundance, we presented the impact of keystone nanocluster concentration on low-temperature k(T) [2,3]. Our study is focused on the As-S glassy systems, where each compound represents a different environment. It is shown that the presence of keystone S_8 nanoclusters leads to the plateau formation in the k(T) of As_2S_3 and As_2S_5 samples. At the same time, the Boson peak in the Cp was preserved, suggesting that nanoclusters contribute to both the k(T) plateau and Cp maximum. Different types of nanoclusters have been previously identified in As-S systems. Each nanocluster can be considered as a separate entity or species. Inspired by the concept of keystone species from ecology, we decided to examine the impact of individual nanoclusters on the low-temperature properties of glasses. The presence of a keystone species is important for maintaining the character of the environment, and without a keystone species presence, the ecosystem would collapse. Combined analysis using two approaches, the Soft-Potential Model and nanocluster approximation, allowed us to identify the exact structure of nanoclusters in a rigid glass matrix responsible for the mentioned universality (Figure 1). The results of this approach are consistent with the experimental data for the case of As-S glasses, and the possible implementation on other glass systems needs to be verified [2,3].

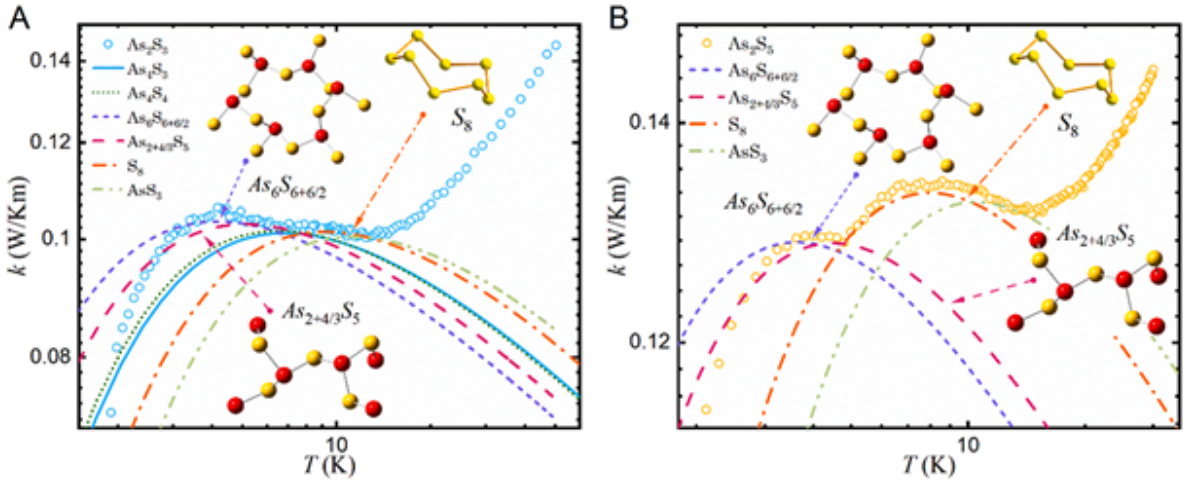

Figure 1. Temperature dependence of thermal conductivity. (A) As_2S_3, (B) As_2S_5 glassy samples. The lines represent an individual contribution from different types of nanoclusters calculated from Soft-Potential Model.

Raman scattering evidence on the correlation of middle range order and structural self-organization of As-S-Ge glasses in the intermediate phase region. — The Raman scattering of bulk nonstoichiometric chalcogenide alloys along the pseudo-binary AsS_3 – GeS_4 tie-line, which completely lies in the intermediate phase (IP) region of As-S-Ge ternary system was investigated in order to reveal the structural transformations in charge of the unusual features of the middle range order, elastic and physical-chemical parameters of these glasses observed earlier [4]. Inside the intermediate phase region chalcogenide glasses, including the As-S-Ge ternary system can form very narrow compositional areas with high level of structural self-organization, mainly due to sudden increase of the concentration of high flexible species (Figure 2).

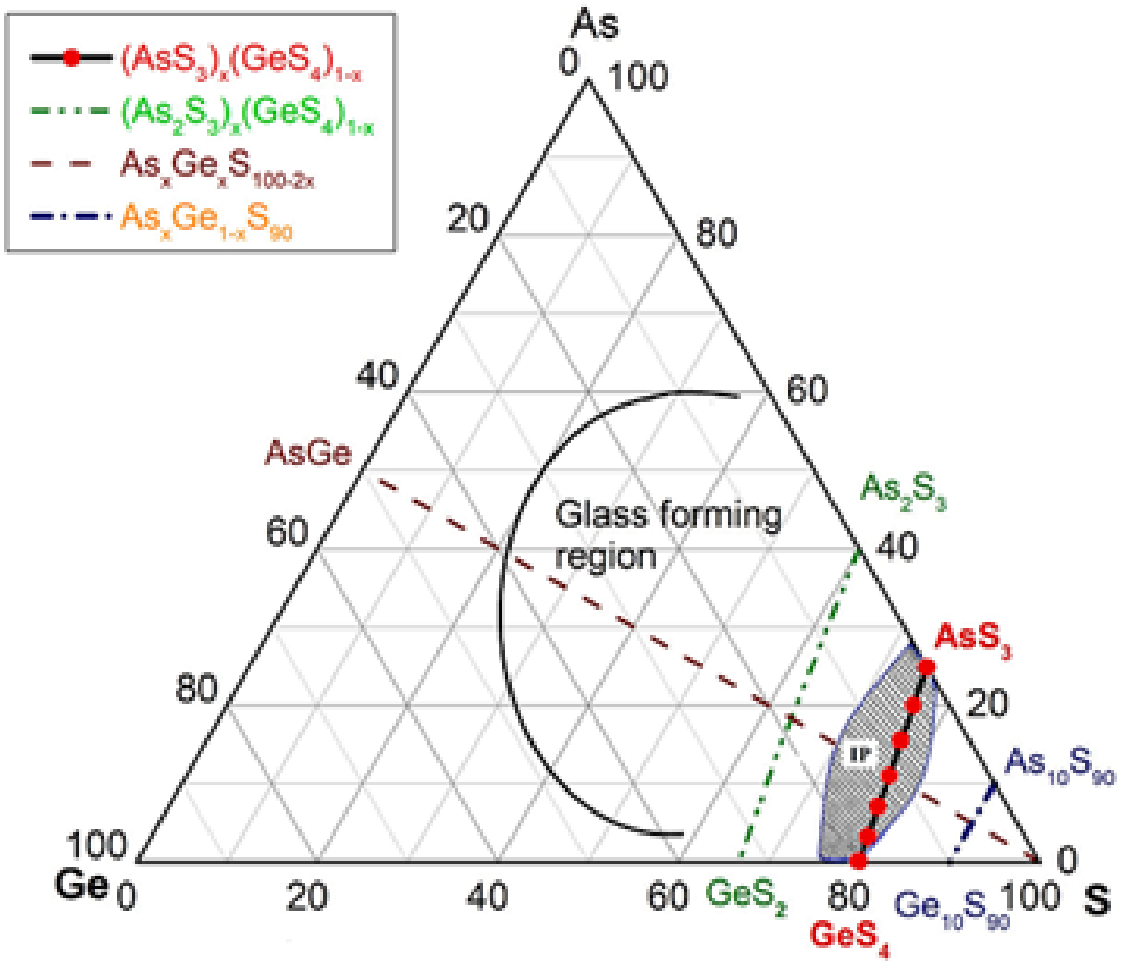

Figure 2. Synthetized AsS_3 - GeS_4 glasses marked by red filled circles. Solid line and hashed area show the glass forming and intermediate phase regions [5] in As-S-Ge system respectively.

Raman scattering measurements were performed to reveal such a compositional area around the composition of $Ge_{7.7}As_{15.3}S_{77}$ (x = 0.33; <r> = 2.31) of the pseudo-binary $(GeS_4)x(AsS_3)_{1-x}$ ternary system. The glasses around this composition appear to be strongly self-organized with an assessed concentration of QT S=As $(S_{1/2})_3$ around 30 % of total atomic clusters being the building blocks of the structure. An evident correlation was observed between the compositional dependence of the Raman scattering normalized strengths, glass middle range ordering (MRO) parameters, molar volume and longitudinal elastic modulus. Around the above mentioned composition corresponding to strong self-organized glass the MRO parameters and the molar volume exhibit global minima, meanwhile the elastic modulus reaches its maximum value [5].

Impact of e-cigarette liquid on porcine lung tissue. — An ex vivo confocal Raman micro-spectroscopy study. — Ex vivo porcine lung immersed in e-liquid was examined using confocal Raman micro-spectroscopy in-depth to evaluate the influence of e-liquid on lung tissue. It was observed that the intensity of lung-related Raman peaks improved after immersed in e-liquid (see Figure 3), which was attributed to the well-known optical clearing effect of glycerol and propylene glycol. Moreover, collagen dehydration was showed by the ratio change of Raman peak intensity (I_{937}/I_{926}) due to influence of the glycerol. We hypothesize that the nicotine free and flavour free e-liquids comprising glycerol and propylene glycol could potentially be employed in clinical protocols as optical clearing agent for improved Raman-guided bronchoscopy in-depth [6].

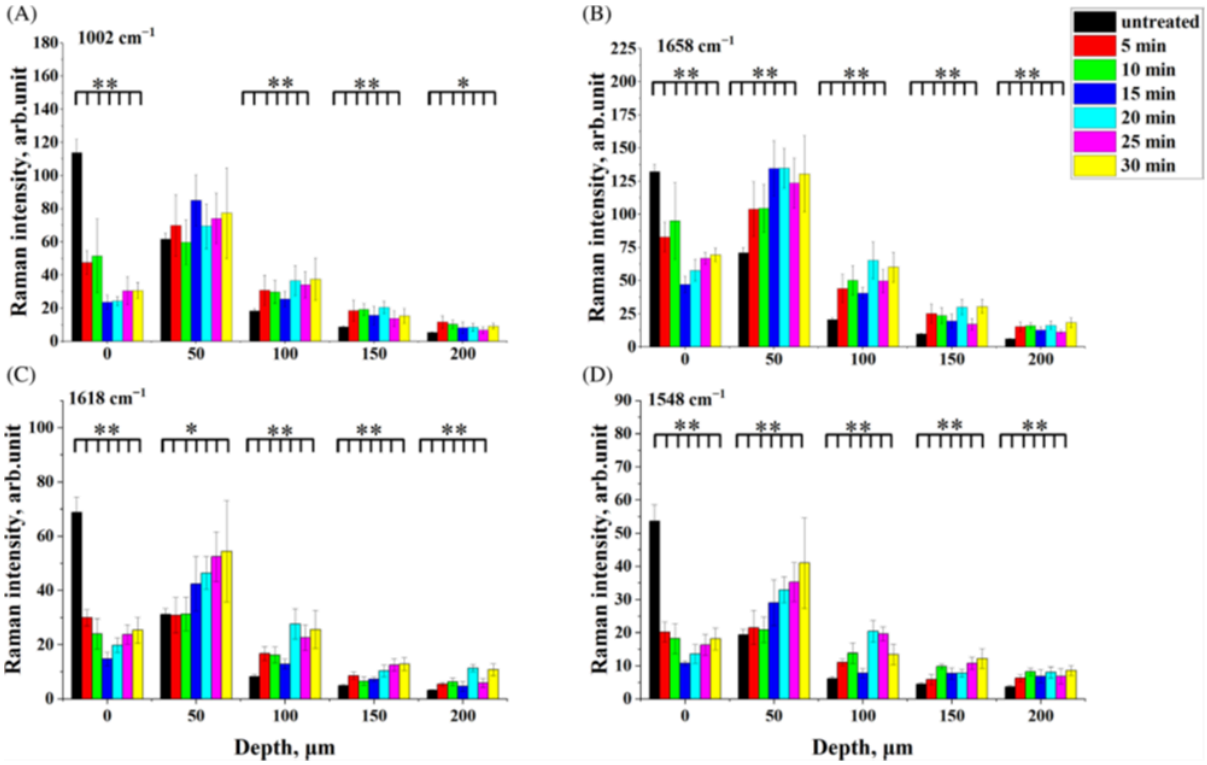

Figure 3. Average intensity of Raman peaks at (A) 1002 cm^{-1}, (B) 1658 cm^{-1}, (C) 1618 cm^{-1} and (D) 1548 cm^{-1} of lung tissue control (black), 5 (red), 10 (green), 15 (blue), 20 (cyan), 25 (magenta) and 30 min (yellow) treatment with e-liquid at various depths from 0 to 200 μm.

Effectiveness of Green Synthesized Zinc Oxide Nanoparticles against Extensively Drug-resistant Klebsiella pneumoniae. — Klebsiella pneumoniae (K. pneumoniae) is a pathogenic nosocomial bacterium developed to be a life threatening factor with high intractable infections. The green route of metal oxide nanoparticles could be a promising treatment option. We developed a sustainable technique of green synthesizing ZnO nanoparticles utilizing the pumpkin seed extract with average size around 68 nm. By mixing the green synthesized ZnO nanoparticles (75 mg) with the culture medium, the K. pneumoniae could not grow suggestion that the green synthesized ZnO nanoparticles could be an important factor to combat the K. pneumoniae and reducing chemical base antibiotic dependency [7].

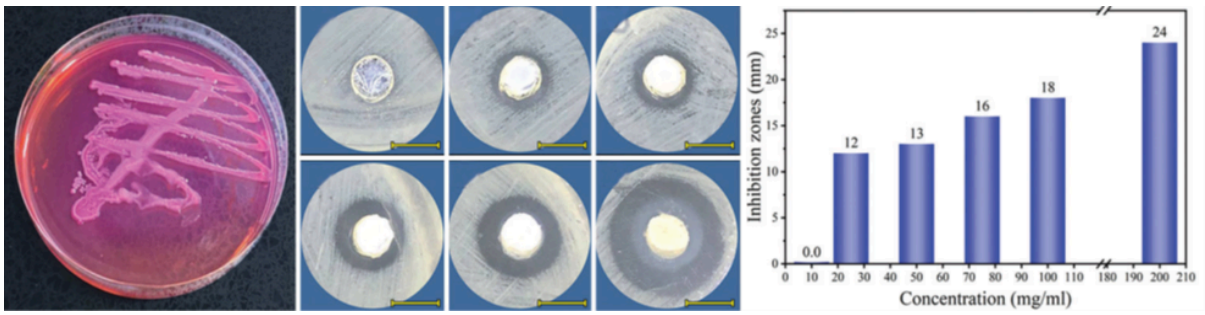

Figure 4. (a) The Klebsiella pneumoniae colony shape, (b g) the antibacterial activity of different concentrations of green synthesized ZnO NPs against K. pneumoniae at 37°C for 1 h, (h) inhibition zone as a function of ZnO NPs concentrations

References:

[1] DOI: https://doi.org/10.1002/pssb.201900525
[2] DOI: https://doi.org/10.1016/j.jnoncrysol.2022.122040
[3] DOI: https://doi.org/10.1063/10.0017815
[4] DOI: https://doi.org/10.1016/j.jnoncrysol.2023.122255
[5] DOI: https://doi.org/10.1002/pssb.202000116

[6] DOI: https://doi.org/10.1002/jbio.202300336
[7] DOI: https://doi.org/10.4103/bbrj.bbrj_167_23

2022

Identification of histidine-Ni (II) metal complex. — Experimental Raman spectroscopy combined with density functional theory (DFT) calculations is useful and non-destructive method to investigate and characterize the metal coordination complexes at the molecular level. The role of metals is becoming increasingly important nowadays, but the growing amount of metals and metal-containing compounds can also lead to potential environmental and health problems. Some metal ions can cause neurological and neurodegenerative diseases, cell damage, and oncogenesis. On the other hand, metal ions play an important role in many biological processes. Therefore, the study of metal complexes in bioligands has received increasing attention in recent decades. For example, the importance of histidine interactions with transition metal ions, including Ni (II), has long been recognized in biological systems. Metal ions such as nickel have a strong binding affinity to amino acids and tends to form the metal complexes of different geometries.

In our study the condition dependent formation of the histidine-nickel (II) complex was examined by Raman spectroscopy. In addition to the experiments, molecular modeling (Figure 1A and 1B) and subsequent DFT calculations on histidine-nickel complexes were performed in order to elucidate the complex formation mechanism and optimal geometry of the structures as well as to facilitate the interpretation of the vibrational spectra. The geometry optimizations and total energy calculations of His-Ni (II) complex revealed that the octahedral geometry and the triplet spin state of Ni ion is the energetically favorable structure.

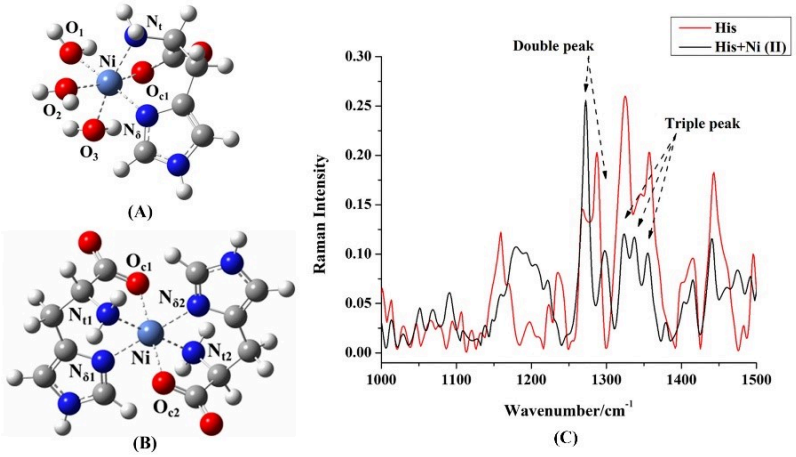

Figure 1. Optimized geometry of gas-phase single (A) and dual (B) histidine-nickel complexes and Raman spectra of His and His-Ni (II) solutions in the range of 1000–1500 cm^{-1} (C).

The Raman spectra of His-Ni (II) solution show characteristic two-peak (at 1272 and 1297 cm^{-1}) and three-peak (at 1322, 1336, and 1355 cm^{-1}) feature that belong to the metal complex (Figure 1C). This complex is formed through the nitrogen atom of the imidazole side chain, the nitrogen atom of the terminal amino group, and the oxygen atom of the carboxyl group. Variation of pH revealed that the alkaline pH favors while the change of the concentration of the metal ions does not affect the His-Ni (II) complex formation. [1]

Study of glycerol diffusivity in ex vivo porcine dura mater by confocal Raman micro-spectroscopy. — Optical clearing (OC) is a promising technique to overcome limitations of light propagation during in-depth studies of different tissues with biomedical imaging. Glycerol is amongst the most efficient optical clearing agents (OCAs) used for optical spectroscopic experiments. In the deeper tissue regions, the OC is affected mainly by the penetration efficiency of the agent. In this study the diffusivity of glycerol was investigated in the framework of a passive diffusion model and water mobility in ex vivo porcine dura mater by confocal Raman micro-spectroscopy in the fingerprint and high wavenumber regions. The penetration of the compound was evaluated by recording the temporal evolution of the characteristic Raman peaks of glycerol and using the Raman peak intensities of the non-movable collagen (proteins) as reference. The results indicate that the collagen-related Raman peak intensities were significantly enhanced for all four depths after glycerol application as illustrated in Figure 2. Moreover, the changes in water concentration after OC treatment indicated that 50% glycerol led to tissue dehydration (see Figure 3). A depth dependence in glycerol concentration and diffusion coefficient was also observed, ranging from 0.6 to 20% and from 9.6 $\times 10^{-6}$ to 3.0 $\times 10^{-5}$ cm^2/s, respectively. This approach can be

used to calculate diffusion coefficient and concentration of other OCAs, such as mannitol and glucose by measuring their diffusion kinetics through the actual concentration in a specific monitoring depth. Additionally, these results, obtained on dura mater, could be transformed to other fibrous biological tissues and organs. [2]

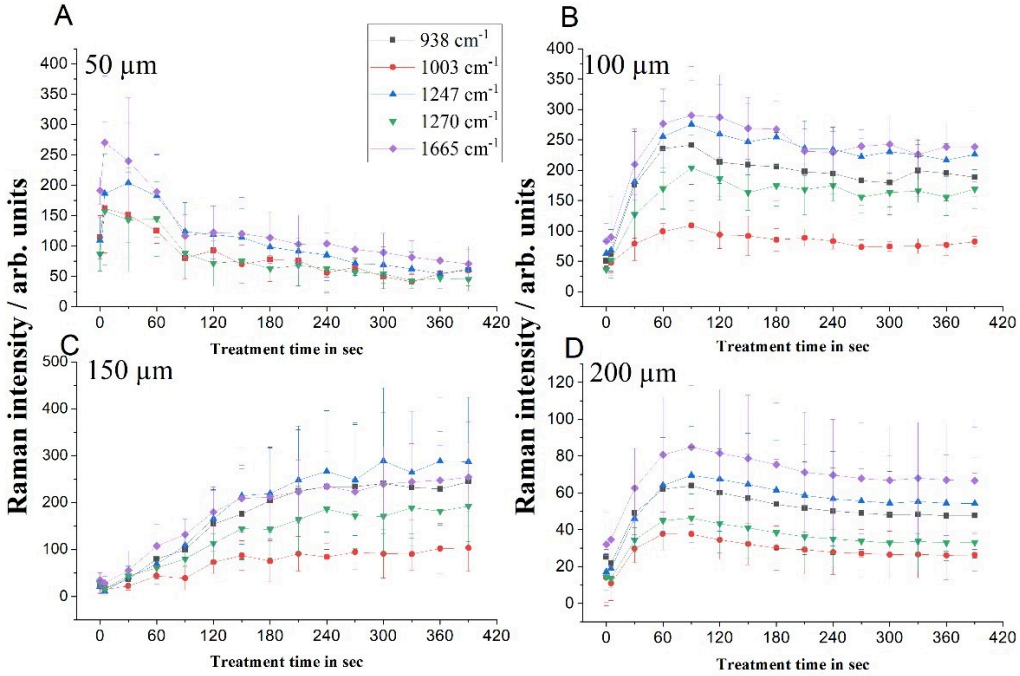

Figure 2. Kinetics of collagen-related Raman peaks at 938 (black squares), 1003 (red circles), 1247 (blue upward triangles), 1270 (green downward triangles), and 1665 cm^{-1} (purple diamonds) in dura mater between 0 and 390 s after treatment with 50% glycerol at different depths of 50 (A), 100 (B), 150 (C), and 200 μm (D).

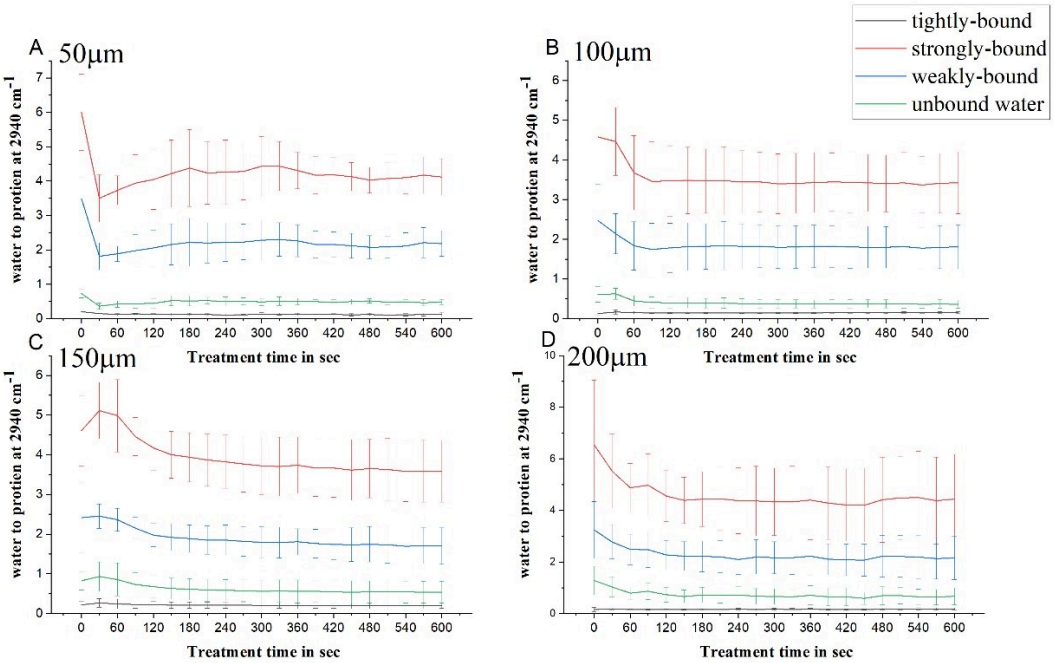

Figure 3. Kinetics of different types of water (tightly bound water (3005 cm^{-1}) – black, strongly bound water (3270 cm^{-1}) – red, weakly bound water (3458 cm^{-1}) – blue, and unbound water (3605 cm^{-1}) – green) in dura mater tissue at different depths of 50 (A), 100 (B), 150 (C), and 200 μm (D). The Raman peak intensities were obtained by the deconvoluted of the water-related Raman band with Gaussians.

Surface-enhanced Raman spectroscopy for the detection of microplastics. — Due to the large occurrence of micro- and nano-sized plastic particles in the environment today, there is an increasing need for a fast and efficient analysis of these particles, and surface-enhanced Raman spectroscopy (SERS) has so far proven to be a convenient, rapid, and simple method for the detection of many chemicals. In this work, a method for detecting

350 nm polystyrene spheres using gold colloids was developed. Gold nanoparticles (Au NPs) of four different sizes were synthesized, characterized, and used as SERS active substrate for microplastic detection. The calculated mean particle size from SEM analysis was estimated to be 33.2, 67.5 and 93.7 nm for spherical samples. The gold nanorod sample has an approximate particle size of 23.5 × 35.5 nm. The influence of different sizes and concentrations of Au NPs on the PS350 SERS signal was investigated, and the nanorod colloid gave the best intensity at 1005 cm^{-1}. After the optimization of the measurement conditions (volume ratio of sample to gold colloid, aggregating agent and its concentration) the detection limit of 6.3 μg/mL was demonstrated, making this SERS-based method sensitive enough for quantitative analysis (Figure 4). The developed technique can be a useful tool for the detection of microplastic pollutants in water. [3]

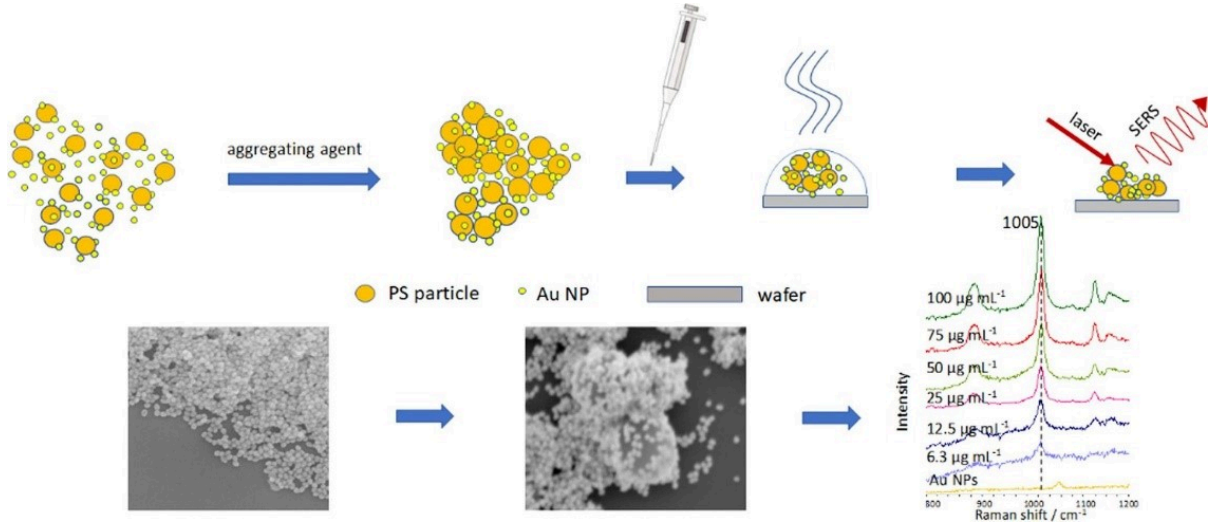

Figure 4. Detection of polystyrene microparticles using the SERS method: schematic diagram of the experimental procedure (top), SEM images of the gold nanoparticles and the plastic microparticle coated with them (bottom left) and the dependence of the Raman spectra on the concentration of the microplastic.

Glyphosate detection by surface-enhanced Raman spectroscopy. — Pesticides are chemical or microbiological agents that control, destroy, repel, or mitigate the effects of various pests such as insects, rodents, and weeds. Unfortunately, their use disrupts the natural balance in the environment, leads to resistance, and can cause water and food contamination. It can also result in their absorption by plants, which are later used in food. While there are strict regulations regarding the maximum concentrations of harmful compounds and additives in food, the control of the production and use of pesticides and the analysis of their presence in food, water, and the environment are expensive and complex. Therefore, it is of great interest to develop simple, rapid, inexpensive, and sensitive methods for the detection of pesticides in samples with low concentrations. Glyphosate is one of the most widely used pesticides in the world. It has been shown to persist in the environment, plants and subsequently in the food. In this work, the detection of glyphosate in low concentrations by surface-enhanced Raman scattering (SERS) using gold and silver nanoparticles (NPs) and three different commonly used laser excitations (532, 632, and 785 nm wavelengths) is compared. In addition, colorimetric detection of glyphosate using cysteamine-modified gold and silver nanoparticles was also tested.

Au and Ag nanoparticles were synthesized and used as SERS substrates. The SERS spectra of different glyphosate concentrations were recorded with Ag nanoparticles at 532 nm excitation and with Au nanoparticles at 632 and 785 nm excitation. The most prominent glyphosate band was found at ≈1036 cm^{-1} (Figure 5). All SERS spectra showed reasonable enhancement of the Raman signal when used for the respective excitation wavelength. The best results were obtained with Ag nanoparticles at 532 nm excitation with a detection limit of 1 mM and with Au nanoparticles at 785 nm excitation with a detection limit of 100 μM.

For colorimetric detection of glyphosate, cysteamine-modified NPs were mixed with different concentrations of glyphosate, and the color change was observed. When cysteamine-modified Au NPs were used, the localized surface plasmon resonance (LSPR) band shifted to higher wavelengths with increasing glyphosate concentration, but when glyphosate was added to modified Ag NPs, the position of the LSPR peak unexpectedly shifted to the blue spectral region. The SERS spectra of glyphosate with cysteamine-modified silver NPs improved the detection limit by two orders of magnitude for 532 nm excitation, i.e., up to 10 μM, and by one order of magnitude for 632 and 785 nm excitation. The broader glyphosate band at ≈1030 cm^{-1} was observed and used to achieve the detection limit of 10 μM for all three excitation wavelengths. [4]

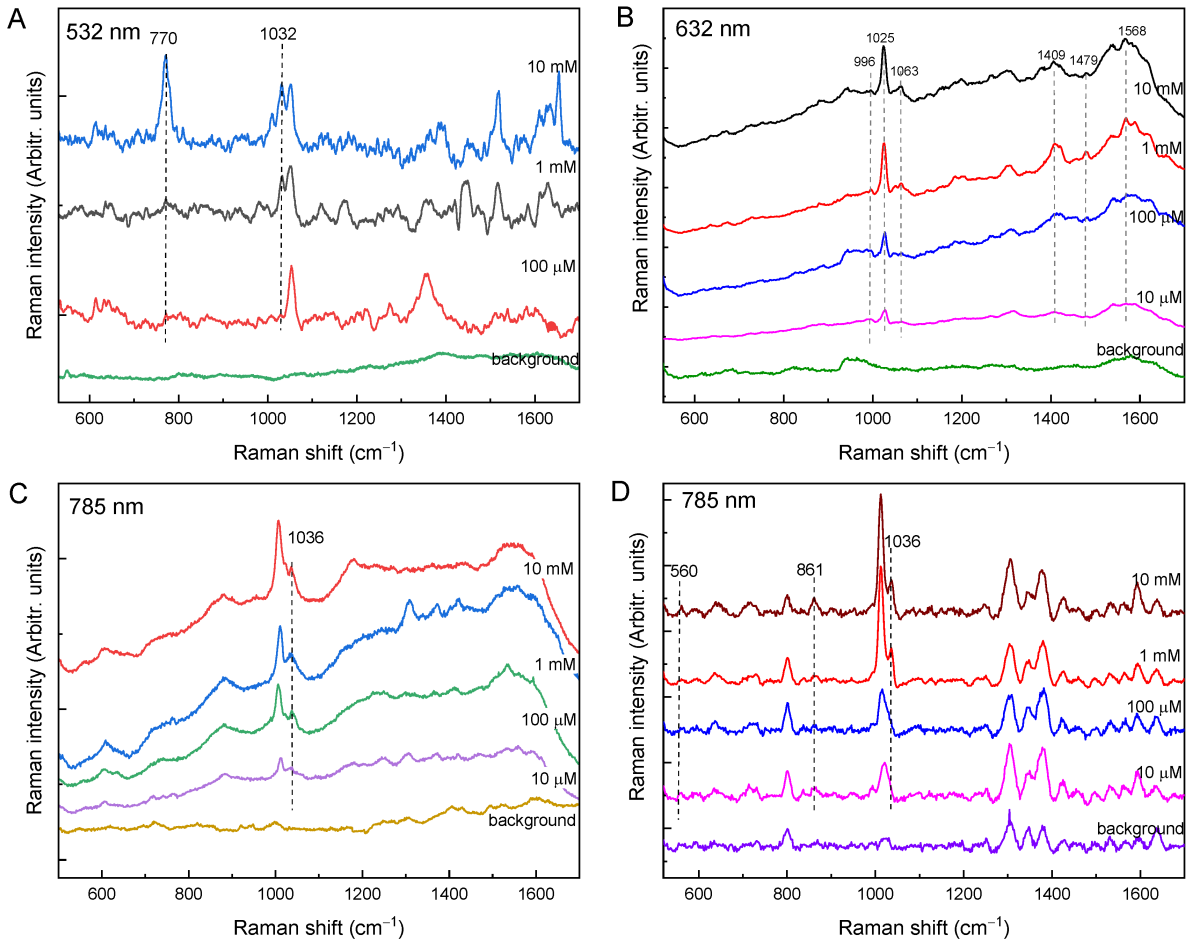

Figure 5. SERS spectra of different glyphosate concentrations: (A) with Ag NPs at 532 nm excitation; (B) with Au NPs at 632 nm excitation; (C) with Au NPs at 785 nm excitation; (D) with Au NPs at 785 nm excitation (baseline corrected; portable Raman).

2021

Diamond color centers. — Due to their superb light emission properties and biocompatibility, color center containing diamond nanocyrstals are promising objects for nanobiology and nanomedicine. These unique structures could be used in a marking and labelling applications, and they are pretended to replace fluorescent dyes which are suffering from photobleaching and photoionization as well as from incompatibility with living organism in some cases. Since the light absorption of tissues and different biological specimens is weaker in the first optical window (600-900 nm), thus highly fluorescent nanodiamond with emission lines lying in this wavelength range are preferred to allow efficient detection of the useful optical signal. Despite of numerous scientific reports, the efficient creation of highly fluorescent nanodiamond crystals of good quality is still challenging. We recently developed an advanced geometry utilizing plasma immersion of impurity source that could significantly increase the color center formation during the MW CVD diamond deposition process. Moreover, our technique allows to use impurity sources, required for desired color center, in solid phase and keep away from laboratory the hazardous gases, commonly applied for this purposes. On the example of silicon vacancy center, we proved that our advanced geometry appropriate to create high quality, SiV center containing nanocrystalline diamond thin films and separated nanocrystals on the silicon substrate with more than 7 times higher zero-phonon line peak intensity as it is possible for impurity source-free geometry.

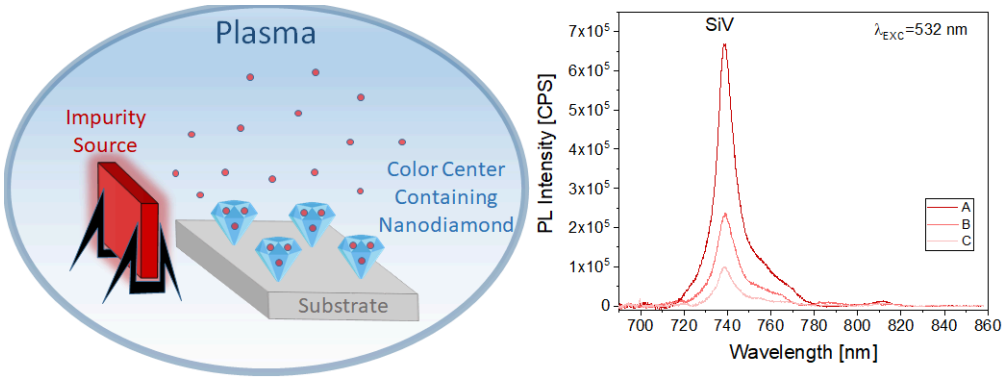

Figure 1. Schematic illustration of the plasma immersed solid impurity assisted growth of the color center containing diamond nanostructures (left). Photoluminescence (PL) spectra of the SiV center containing nanocrystalline diamond films deposited at different conditions (right): A – advanced geometry when an additional Si impurity source is immersed into the CVD plasma; B – a Si impurity source of the same dimensions placed next to the substrate; C – configuration without additional Si impurity source. The PL spectra were recorded at the same conditions using 5 mW incident power of a 532 nm diode pumped solid state laser.

Porous silicon-based nanoparticles for surface enhanced Raman spectroscopy. — Surface-enhanced Raman spectroscopy (SERS) is an emerging vibration spectroscopy technique nowadays. The key to its high sensitivity is the fabrication of metallic nanoparticle-based plasmonic structures capable of efficient amplification of the Raman signal. Porous Si (PSi) nanoparticles (NPs) were prepared by magnesiothermic reduction of the synthesized SiO_2 spheres, and Ag NPs were deposited on the PSi with formaldehyde or HF (Fig.2a) [1]. In addition, silver NPs were deposited on the porous Si obtained by milling and etching the Si wafer. Silver NPs on SiO2 spheres and particles with Ag core and mesoporous SiO_2 shell were also synthesized (Fig.2b). SEM analysis showed the Ag NPs size distributions between 30.1 and 64.3 nm. The synthesized samples were quite stable in aqueous media and had zeta potential between –11.5 and –44.3 mV. The samples exhibited reversible physisorption isotherms of type II except for the sample with Ag core and SiO_2 (Ag–S) coating, which exhibited a type IVa isotherm with the hysteresis characteristic of mesoporous adsorbents. The BET surface areas of the samples ranged from 9 to 56 m^2g^{-1}, with the mesoporous Ag–S sample having the largest surface area of 378 m^2g^{-1}. The surface enhanced Raman spectroscopy (SERS) performance of the synthesized samples was studied by analysing the detection limit of 4-mercaptophenylboronic acid (4-MPBA) as a probe molecule at 532 nm laser excitation. The lowest limit of detection of 1×10^{-5} mol dm^{-3} was obtained with the sample in which silver NPs were deposited on silica spheres (S–Ag) (Fig.2c).

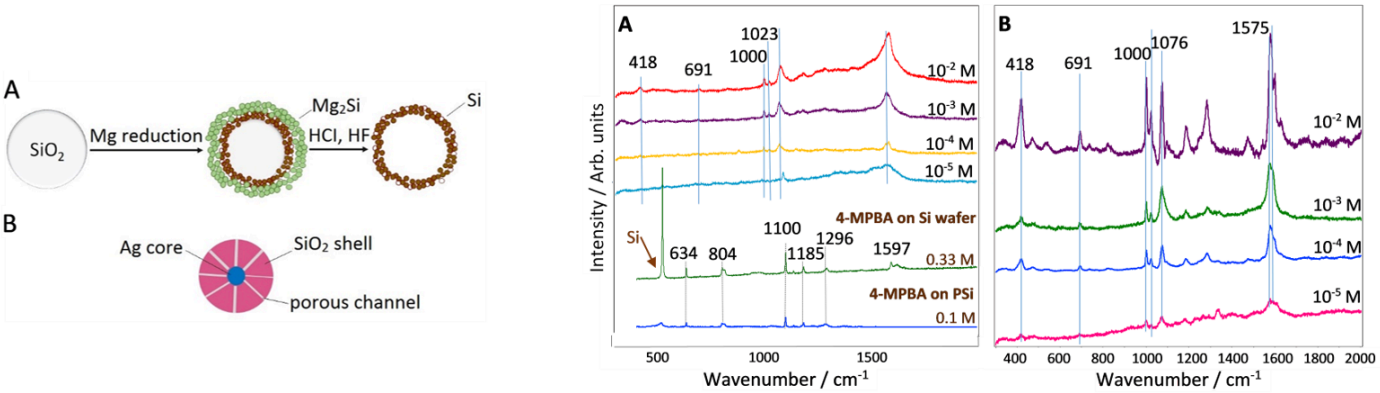

Figure 2. Schematic illustration of a) porous Si formation from synthetic SiO_2, b) NP with Ag core and SiO_2 coating, and c) SERS spectra of different 4-MPBA concentrations on Ag NPs on the surface of SiO_2 spheres (S-Ag).

Confocal Raman micro-spectroscopy of porcine tissues with optical clearing. — Confocal Raman micro-spectroscopy (CRM) combined with optical clearing (OC) technique was used for in-depth study of the collagen in ex-vivo porcine skin in the Raman fingerprint region. The OC technique and CRM allowed one to preserve the high probing depth, signal-to-noise ratio and spectral resolution simultaneously. It was shown that the principal Raman peak intensities of skin are significantly increased at all observed depths after applied glycerol treatment for 30 min and 60 min as an optical clearing agent (Fig.3).[2]

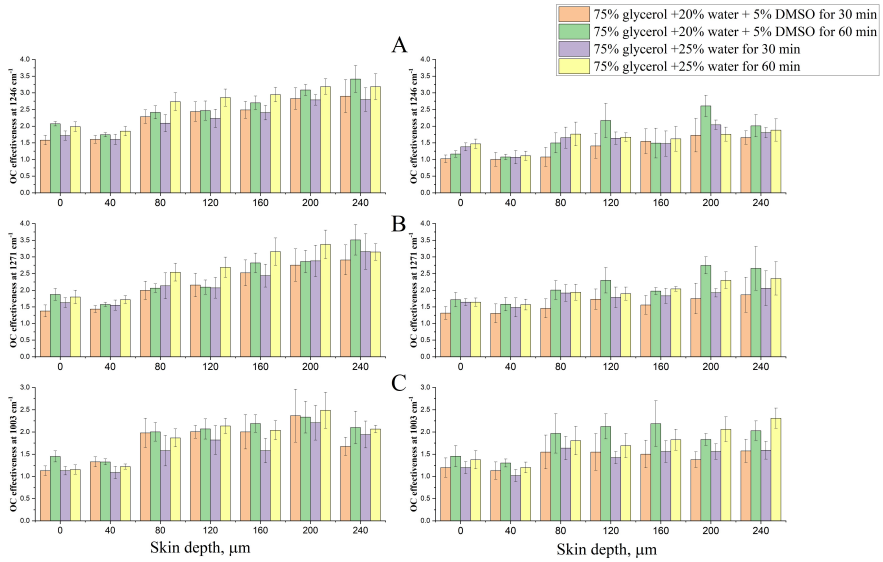

Figure 3. Optical clearing effectiveness for the porcine skin treated by different OCAs for different exposure times of 30 min and 60 min for the Raman peaks at (a) 1246 cm^{-1}, (b) 1271 cm^{-1} (amide-III region) and (c) 1003 cm^{-1} (phenylalanine/urea) recorded with 785 nm (left) and 633 nm (right) excitation.

The influence tissue optical clearing on ex vivo confocal Raman microspectroscopy (CRM) was assessed also in porcine dura mater in order by to increase the in-depth probing of the collagen. Raman intensities were significantly increased at the depth of 250 μm after treatment with glycerol as the OC agent. The results showed that the OC can be divided into three main steps. The first one is a fast process of tissue dehydration accompanied by collagen shrinkage while the second relatively slow process is related to the glycerol penetration into the interfibrillar space of collagen combined with swelling of tissue. The third step is collagen dissociation caused by the high concentration of glycerol (Fig.4).[3]

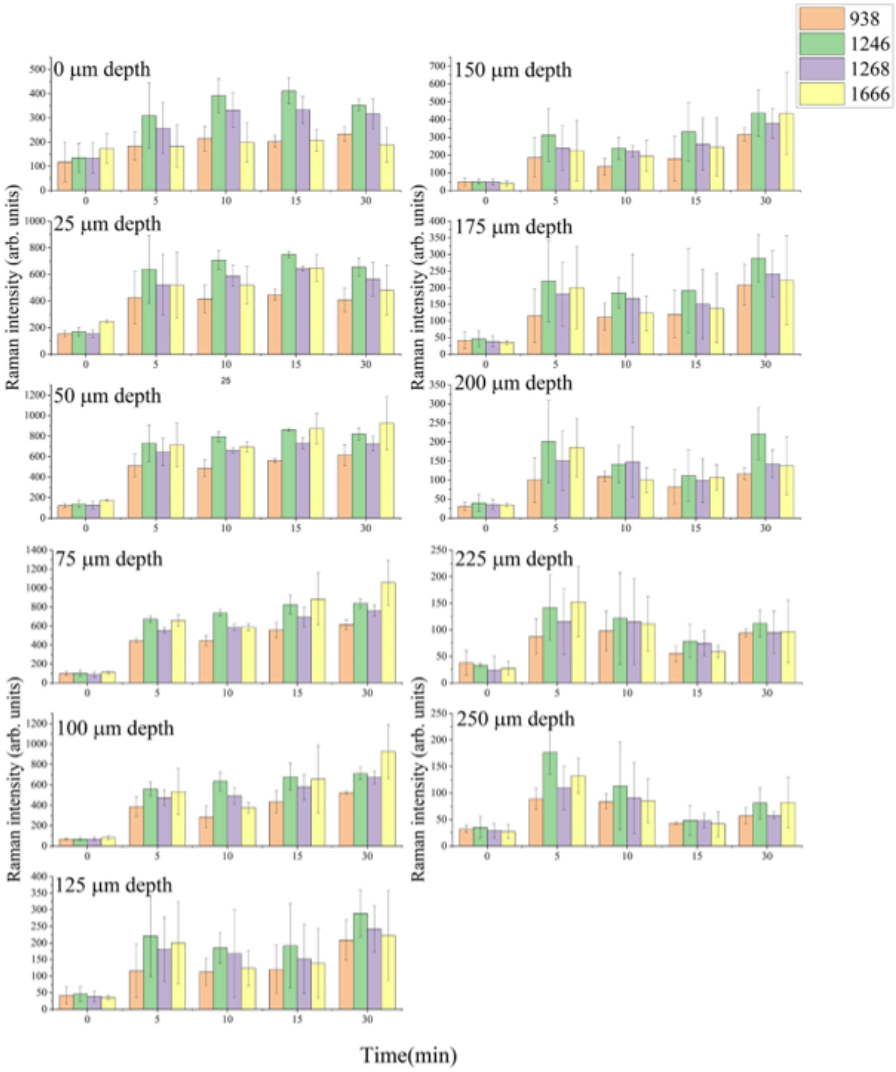

Figure 4. Evolution of the Raman bands of dura mater at 938, 1246, 1268, and 1666 cm^{-1} with depth between 0 and 250 μm with time, after the application of 99.0% glycerol as optical clearing agent.

Raman spectroscopic study of the degree of conversion during gamma-radiation initiated polymerization. — Diethylene glycol dimethacrylate (DEGDMA) is a biocompatible polymer forming highly crosslinked structure that is widely used in dentistry and high-pressure liquid chromatography columns. Gamma radiation-initiated polymerization is a simple and efficient technique to prepare DEGDMA polymers of different size and shape, requiring monomer mixture containing the solvent and the monomer only. In addition, bulk structures ranging from non-porous to macroporous character can be obtained changing only the type and the amount of the solvent. The degree of conversion of diethylene glycol dimethacrylate monomer in different solvents upon gamma irradiation with different doses have been studied by Raman spectroscopy and mass difference measurements (Fig.5). It has been shown that the Raman method allows determining the conversion rate of monoliths by a non-destructive and, in terms of realization, simple manner. A good agreement was found in the degree of conversion determined by Raman spectroscopy and mass difference-based techniques. The data were fitted with the Avrami equation and the observed differences in the reaction rate were explained by the different character of the DEGDMA polymerization mechanism in alcohols and other types of solvent, caused by their solubility values. It was found that the degree of conversion for DEGDMA reaches a plateau by increasing the irradiation doses and it exceeds 90% above 12 kGy, independently of the applied solvents. Raman measurements revealed also that there are DEGDMA monomers entrapped intact into the polymer matrix and/or attached to the frame only through the methacrylate group [4].

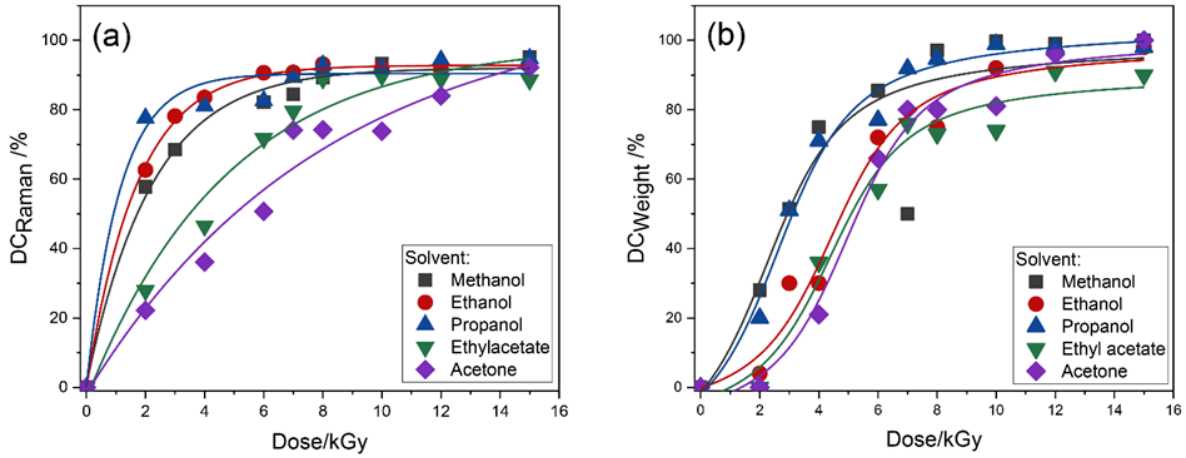

Figure 5. Degree of conversion of different DEGDMA/solvent systems with applied dose determined from (a) Raman peak intensity ratios and (b) weight difference measurements. The solid lines are curves of the Avrami fitting.

2020

Analysis of lithiated silica glasses by laser induced breakdown spectroscopy and Raman spectroscopy. — Conducting lithium glass materials are promising candidates for electrolytes of next generation batteries. Increasing demand for rechargeable batteries for electromobility and grid storage applications has exposed shortcomings of traditional lithium-ion technology such as safety and environmental issues. Lithium-aluminosilicate glass ceramics exhibit a range of exciting properties that can be commercialized in various ways. Nearly zero thermal coefficient (and thus extreme resistance to heat shock) combined with transparency are very favorable for applications such as domestic cookware and precision optics. In addition, a low dielectric constant makes β-spodumene glass ceramics promising materials for packaging of integrated circuits [1].

Composition and bonding configuration of silicate glasses with different lithium content was studied by laser induced breakdown spectroscopy (LIBS) and Raman spectroscopy. The lithium content of the formed glass matrix has been determined by using LIBS with high precision. The analysis of the series of LIBS spectra measured on lithiated silica glasses showed that lithium has two spectral lines suitable for the analysis: at 610.4 nm and at 670.8 nm. The former is less intense and located only 0.1 nm away from the calcium line at 610.3 nm (Figure 1a). This makes the spectral line at 670.8 nm a better choice for the analysis, promising higher limits of detection and more accurate quantification.

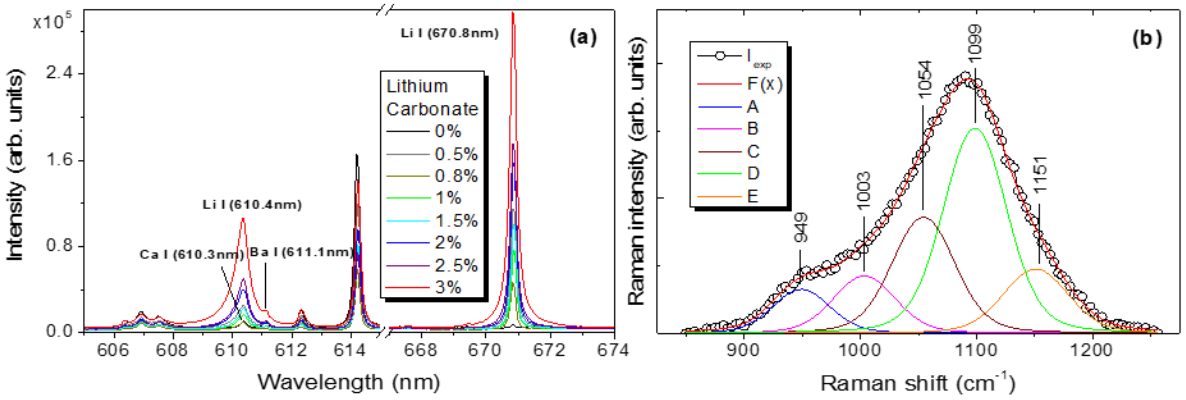

Figure 1. *Comparison of lithium lines at 610.4 and 670.8 nm in the LIBS spectra of lithium containing glass samples (a) and decomposition of the 960/1090 cm^{-1} Raman band of the sample with 0.0 wt% Li content by fitting with five Voigt functions (b).*

The broad feature around 1090 cm^{-1} in the Raman spectra of lithium containing samples has a complex shape and can be decomposed into several components. Five subcomponent bands can be assigned to the specific [SiO_4] tetrahedron Q^n structural units with different number of 'non-bridging oxygen' atoms: Q^0 (SiO_4^{4-} monomer),

Q^1 ($Si_2O_7^{6-}$ dimer), Q^2 (SiO_3^{2-} chain), Q^3 ($Si_2O_5^{2-}$ sheet) and Q^4 (fully polymerized three-dimensional SiO_2 network) [2,3]. Figure 1b shows the spectral decomposition illustrated on the spectrum of the 0.0 wt% Li sample, including the components (five bands, A-E, correspond to the Q^0-Q^4 structural units, respectively), the fitted and the experimentally measured curves [4]. Analysis of the Raman spectra implied on the complex character of lithium incorporation into the glassy matrix with lithium content. It was found that the addition of lithium results in more depolymerized SiO4 structures and, in general, increases the disorder of the structure. However, at certain concentrations lithium has an ordering effect due to more homogeneous size distribution of structural units of the glass matrix.

Periodic structures for plasmonic enhancement. Periodic arrays of inverse pyramids with characteristic size of a few micrometers were among the first SERS active substrates finding commercial utilization. Recently we found that the insertion of a gold nanoparticle (GNP) into the inverse pyramid remarkably increases the near-field enhancement (NFE) properties of the structure. Our results showed that the near-field intensity distribution depends on the size of the nanoparticle [5]. The NFE of the inverse pyramid array can further be improved by introducing nano-roughness to the gold surface, for example, by laser ablation.

This effect of this surface treatment on the near-field intensity (E) distribution in inverse pyramids was studied by finite-difference time-domain (FDTD) calculations performed on the same micrometer sized gold coated inverse pyramid with flat and rough surfaces. The dimensions of the structure and the surface roughness value were taken from experimental data obtained on real gold coated substrates. It was found in the presence of roughness the maximum near field intensity increases by 20%. Converting this to E^4 values characterizing plasmonic surface enhancement and NFE properties of the substrate, it can be concluded that the increase of the latter is almost 10^4 [6].

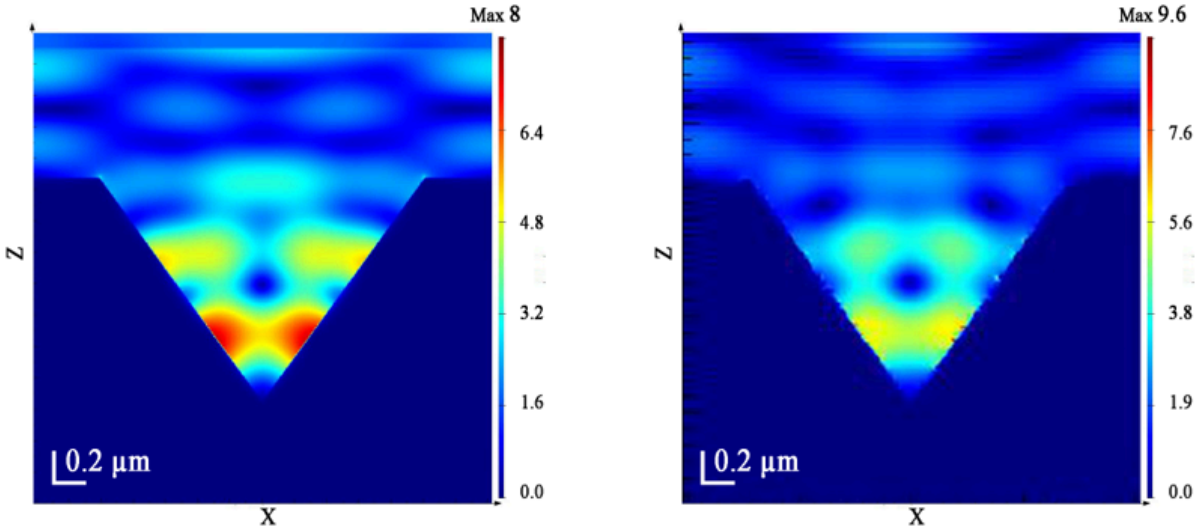

Figure 2. *Near-filed intensity distributions of inverse pyramids with flat and rough surfacea.*

2019

Color centers in nanodiamond. — Diamond nanostructures containing optically active point defects or so called “color centers” have attracted attention of many researchers in last decades. These unique nanoobjects with excellent physical and optical properties are very promising candidates for novel photonic and biological applications, including but not limited to room temperature solid state single-photon source, extremely sensitive magnetometry, nanoscopy, biocompatible labeling or drug delivery systems. Most of the mentioned applications are based on the superb photoluminescence (PL) properties of this diamond-based nanosystem among which the zero-phonon line (ZPL) peak postion, intensity and spectral shape are the most important characteristics.

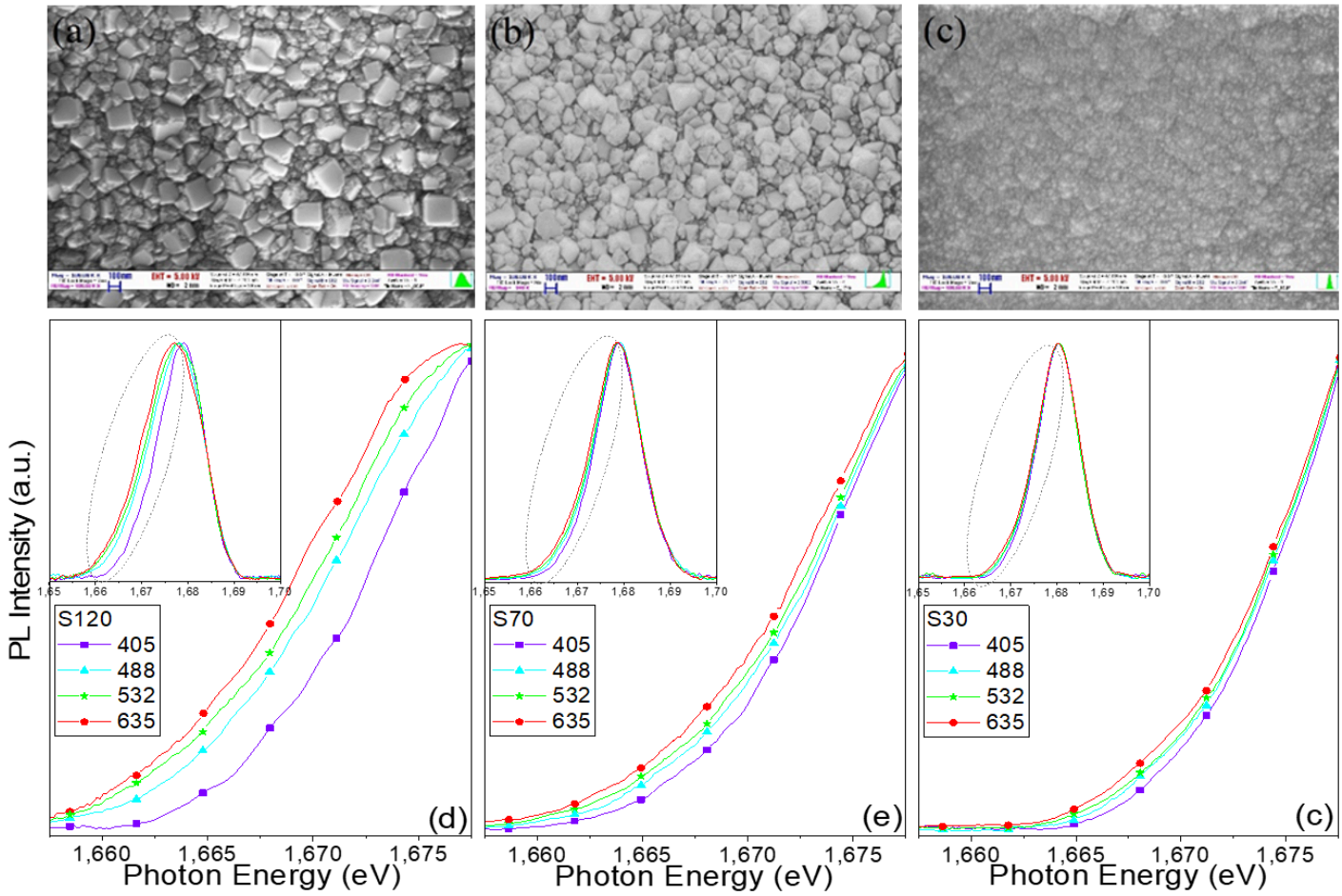

Figure 1. *SEM micrographs of nanocrystalline diamond thin films with average grain size of (a) 120, (b) 70 and (c) 30 nm (top) and the differences in their ZPL line shape revealed by applying laser excitations of 405 (3.06 eV), 488 (2.54 eV), 532 (2.33 eV) and 635 (1.95 eV) nm (bottom). The full ZPL emission spectra are shown in the inset. All PL spectra were recorded at room temperature.*

The asymmetric line shape in form of an elongated tail on the low energy side of the ZPL was studied in detail for silicon-vacancy (SiV) center being a very strong candidate for above mentioned applications. By applying multi-wavelength excitation PL spectroscopy, significant differences in the spectral line shape were observed in case of the SiV center containing chemical vapor deposited (CVD) nanocrystalline diamond thin films having different grain sizes (Fig. 1). The PL measurements revealed that the SiV center related 1.68 eV PL line shape sensitive to the excitation energy, and the asymmetric tail on the low-energy side of ZPL becomes more pronounced with decreasing of the excitation energy. The asymmetry of the 1.68 eV PL line was found to be stronger in the samples containing larger diamond nanocrystals and it was attributed to the luminescence contribution of the simplest point defect in the diamond lattice, which builds up by a vacant single carbon site, namely to the GR1 center, being simultaneously presented in the structure. The varying degree of the ZPL asymmetry with the average grain size of the nanodiamond films was explained by the preferential environmental condition for the GR1 defect formation process.

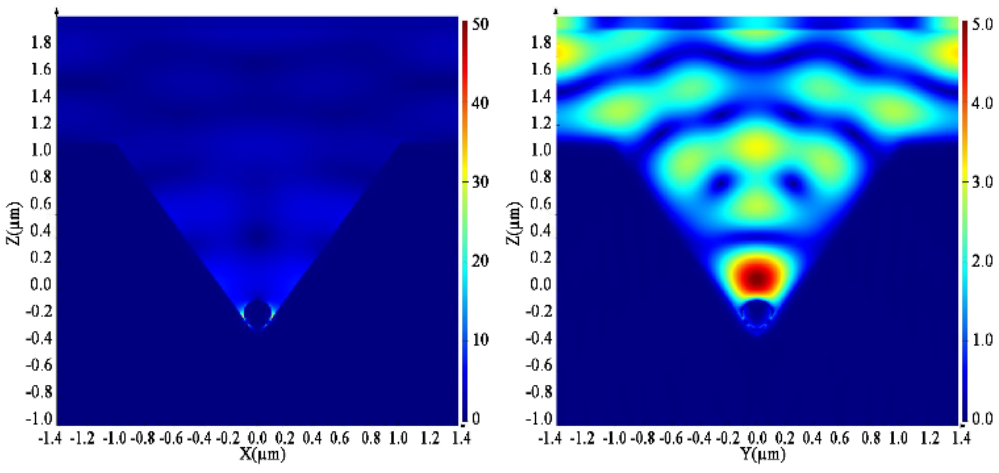

Figure 2. *Calculated distributions of near-field intensity (E) inside an inverse pyramid with 2 microns base entrapping a gold nanosphere of 200 nm diameter.*

Plasmonic amplification in hierarchically combined micro- and nanostructures. — Being a non-contact, fast and relatively easy material characterization technique requiring no sample preparation, Raman spectroscopy is finding many applications in biology, life sciences and other areas. However, the effect is relatively week, but it can be enhanced with different techniques, like surface enhanced Raman scattering (SERS), where the incident or scattered light is enhanced by the interaction with localized electron oscillations on metallic surfaces (plasmons). In SERS the enhancement of the plasmonic surface has two origins: one – usually weaker – comes from electrochemical phenomenon, the other – from electromagnetic interaction. The material, shape, symmetry, orientation, surrounding media are the most important factors affecting the amplification. In case of core-shell structures the inner diameter and layer thickness ratio are also crucial. In addition, surface functionalization can be used to achieve selective enhancement of specific target molecules.

Lithography and nanotechnology allow to fabricate hierarchically combined micro- and nanostructures with advanced SERS properties . In cooperation with the MEMS lab of the Institute of Technical Physics and Materials Science, Centre for Energy Research, novel SERS substrates have been developed capable of entrapping and Raman characterization of different molecules . Functional groups of human blood and parvovirus were identified with this technique . In addition, giant SERS enhancement was discovered in SERS substrates consisting of inverse pyramid entrapping gold nanoparticle. The results of modelling performed with finite-difference time-domain method showed that the near-field intensity distribution has extreme maximum in the small voids around the contact points of the nanosphere and pyramid surface (Fig. 2) .

Nano-gold catalyzed synthesis of novel As-S crystallites. — Due to the advantageous combination of infrared transparency, optical activity, structural photosensitivity and high level of third-order optical non-linearity amorphous and crystalline chalcogenides attract significant attention in modern optoelectronics and photonics. They offer wide possibilities for modern applications as a media for optical data storage, optical signal processing, photolithography, thermal imaging, molecular bio-chemical sensing, solar cells, solid electrolytes, bioscience and medical applications, etc. Most of the physico-chemical properties of chalcogenides are determined by their nanoscale structure , . Among different compositions in the As-S system, several compounds such as duranusite (As_4S), α- and β-dimorphites (As_4S_3), α-, β-realgar and pararealgar (As_4S_4), uzonite (As_4S_5), alacranite (As_8S_9) and orpiment (As_2S_3) are known as minerals.

A novel method has been developed to prepare As-S chalcogenide crystals by gold-catalyzed thermally initiated chemical vapor deposition. Different sizes (5, 20, 40 and 60 nm) of gold nanoparticles were used in order to activate the catalytic reaction. Crucial differences were observed between these structures and those prepared by the well-known thermal deposition of As-S chalcogenide films. The latter were found to contain large concentrations of photosensitive realgar-like As_4S_4 and As_4S_5 inclusions in comparison with the structure of bulk As_2S_3 glass. In contrast, the growth of molecular nanocrystals was observed on the surface of films obtained with the gold-catalyst assisted method. The size and shape of crystallites on the surface of As-S films weredefined by scanning electron microscopy. Depending on synthesis conditions, these crystallites are built from different cage-like molecules. The surface enhanced Raman spectra of crystallites together with the results of density functional theory calculations let us identify As_4S_5 and realgar-type As_4S_4 cage-like molecules forming tetra-arsenic pentasulfide (uzonite) and tetra-arsenic tetra-sulfide (realgar) crystals, respectively. The uzonite structure was found to be insensitive to laser irradiation while photo-structural transformation was observed for the latter in a result of laser exposure (Fig. 3).

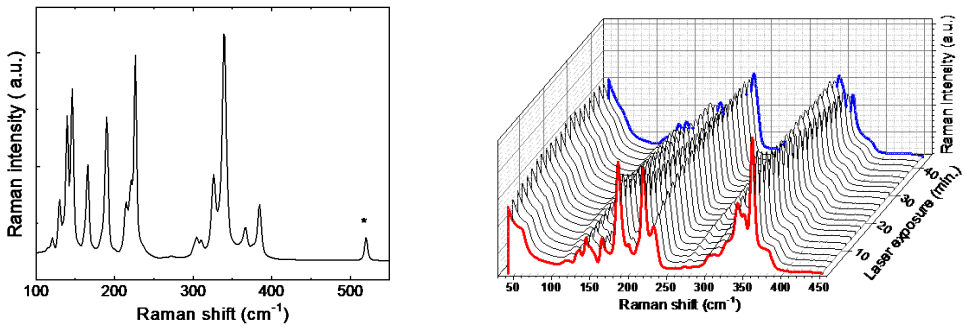

Figure 3. *Raman spectrum of As_4S_5 crystallites prepared with nano-gold catalyst (left). In-situ photostructural transformation (realgar-pararealgar transition) of As_4S_4 (realgar type) crystallites prepared with nano-gold catalyst, measured by Raman spectroscopy (right).*

2018

Gold-catalyzed synthesis and structural characterization of a new type of As-S nanocrystallites. — Non-crystalline chalcogenides with high infrared transparency have stood out as materials of choice for infrared optics. Detailed study of the physical properties of these materials revealed their unique and remarkable structural, electronic, optical properties and large functionality, and has attracted significant attention, representing an important scientific and technological challenge as well. They offer wide possibilities in domains such as information technologies (optical data storage, ultrafast optical transmission and information processing), photolithography, renewable energy technologies (high efficiency solar cells, solid electrolytes), medicine, thermal imaging, sensing and biosensing etc. Recent progress in photonics shows that amorphous chalcogenides are among the best candidates as active optical media for ultrafast all-optical processing systems.

Crucial differences were observed between structure and properties of As-S chalcogenide thin films prepared by normal and gold-catalyzed thermally initiated vapor deposition from the same As_2S_3 glass precursor. The as-deposited As_2S_3 film prepared by thermal evaporation contains large concentrations of photosensitive realgar-like As_4S_4 inclusions compared to the structure of bulk As_2S_3 glass. The irradiation of this film by near- or over-bandgap coherent light initiates significant structural transformations connected mainly with induced transformation of realgar As_4S_4 molecules into their pararealgar polymorph. In contrast, formation of novel molecular nanocrystals was observed on the surface of As_2S_3 films synthesized with gold-catalysis. The size and shape of the crystallites was characterized by electron microscopy and their structure was found to be not photosensitive. Surface enhanced Raman spectra of crystallites were interpreted with DFT calculations and showed that the crystallites are built from As_4S_5 cage-like molecules forming tetra-arsenic pentasulfide (Figure 1).

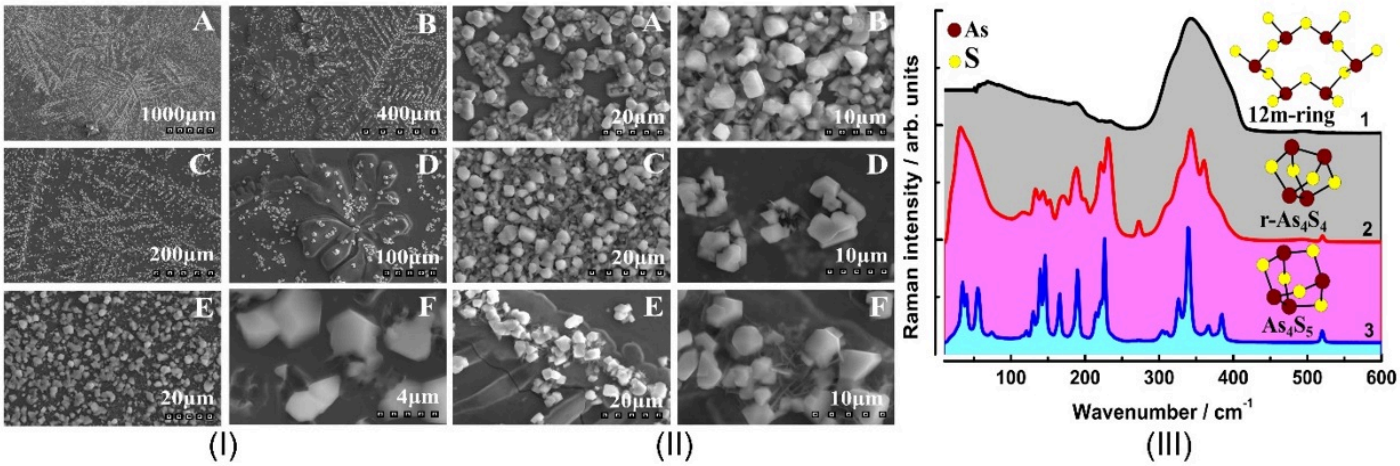

Figure 1. *(I) Surface morphology and distribution of As_4S_5 micro-crystallites on As_2S_3 films synthesized by gold-catalyzed vapor deposition on 5-60 nm Au nanoparticles (A-F); (II) SEM images of As_2S_3 nanolayers synthesized with spherical gold nanoparticles of different size: 5 nm Au-np (A,B), 40 nm Au-np (C,D), and 60 nm Au-np (E,F); (III) FT-Raman spectrum of glassy As_2S_3 (1) and surface enhanced Raman spectra of As-S thin films prepared by thermal deposition (2) and gold-catalyzed vapor deposition (3). The main clusters constituents of the films are also indicated on the Figure.*

Color centers in nanodiamond. — A gold-coated array of flow-through inverse pyramids applicable as substrate for entrapment and immobilization of microobjects and for their subsequent surface enhanced Raman spectroscopic (SERS) characterization was fabricated using bulk micromachining techniques from silicon. The inverse pyramids have 2.2x2.2 microns sized base on the top (being flush with the silicon surface) and a 0.5x0.5 microns sized opening on the bottom (Figure 1). The perforated periodic 3D structure was demonstrated for parallel particle trapping and sensitive detection of molecules by entrapment and SERS characterization of polymeric microspheres. It was found that the periodic array has efficient near-field enhancement in the 650-850 nm region. Raman intensity maps recorded over the entrapped microspheres indicated efficient SERS enhancement inside the inverse pyramids.

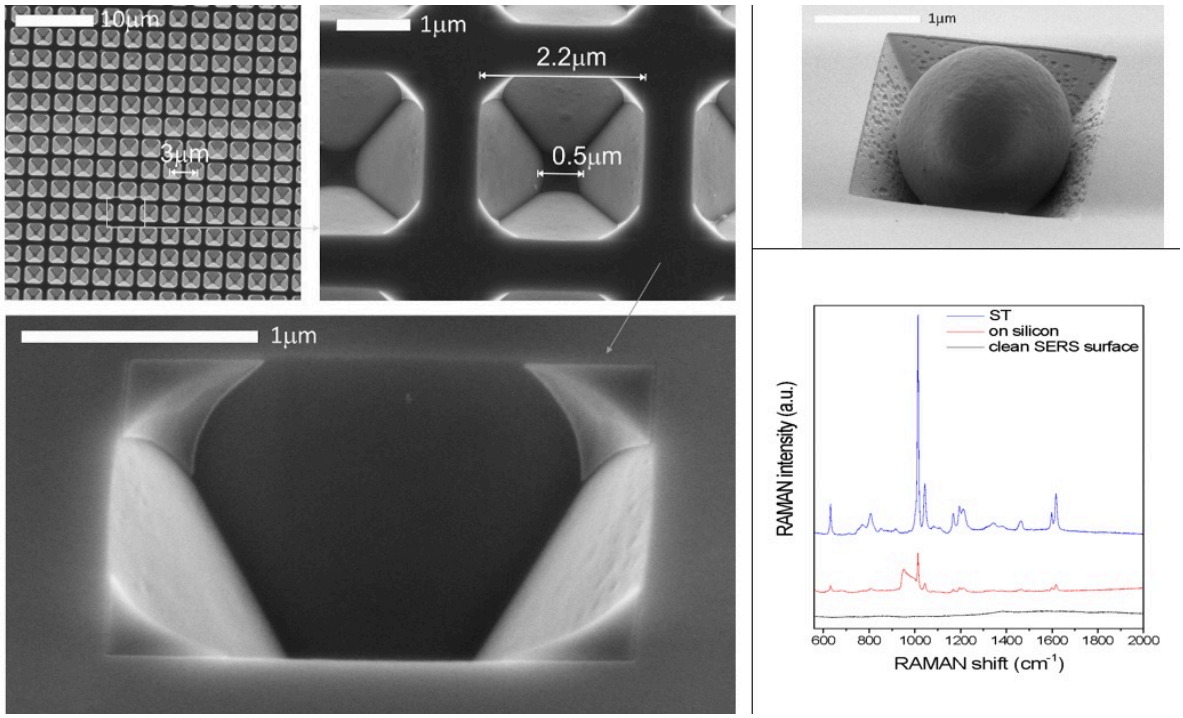

Figure 1. *SEM view of the periodic perforated SERS substrate applicable for flow-through experiments and particle and cell entrapment (left). Polymeric microparticle entrapped in an inverse pyramid of the SERS substrate (top right). Comparison of the SERS spectra recorded on the clean SERS surface and entrapped microparticle (ST) and normal Raman spectrum of the latter on silicon (bottom right).*

2017

Color centers in nanodiamond. — Among the numerous optically active defects (color centers), studied in nanosized diamond (ND), the silicon-vacancy (SiV) center is a promising candidate for utilization in different fields like quantum computing and cryptography, nanoscopy, medicine or cell biology. Most applications are based on the intensive and narrow zero-phonon emission line (ZPL) of the mentioned color center, which can be detected in near infrared wavelength region, around 1.68 eV (738 nm). However, the asymmetric lineshape of the SiV ZPL may restrict the spectral parameters important for different applications and prohibit the determination of the real ZPL characteristics by traditional spectroscopic techniques.

Micro-photoluminescence measurements performed on a high number of CVD nanodiamond films containing SiV centers showed that the undesirable asymmetric tail on the low-energy side of the ZPL is related to another optically active defect (so-called GR1 center) being present in the nanodiamond structures as well. Regions with relatively high GR1 content and with well-distinguishable zero-phonon lines related to different optically active defect structures can be localized by mapping of the ND film with an appropriate excitation wavelength (Fig. 1).

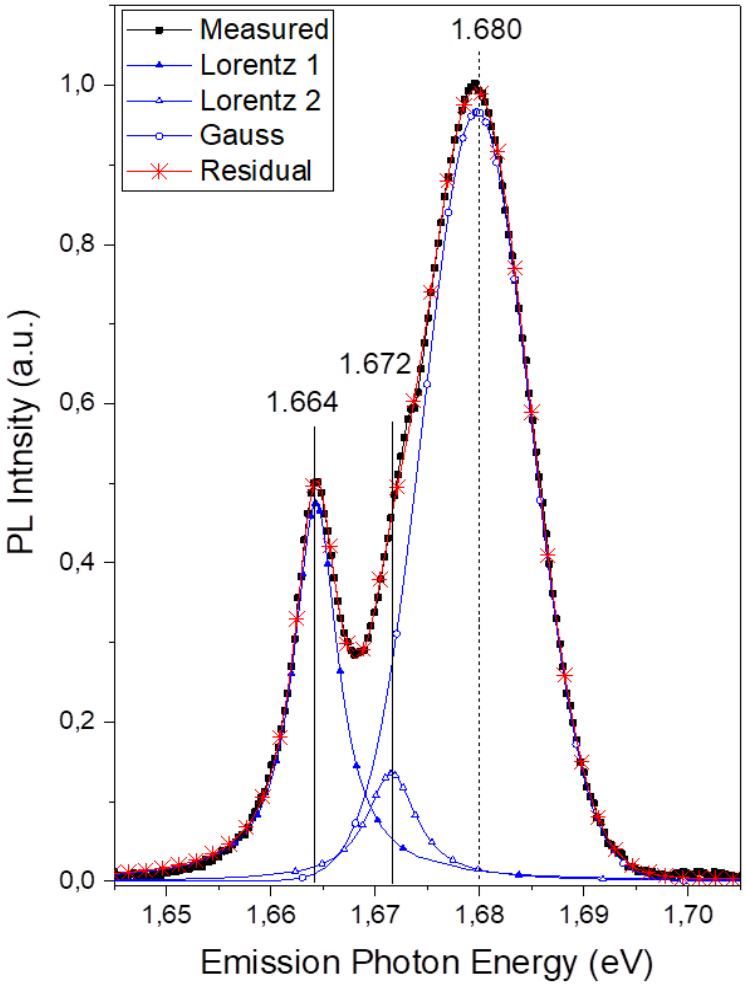

Figure 1. *Fine-structured emission spectrum of CVD nanodiamond film around the SiV center ZPL region excited by 635 nm and recorded at room temperature. The deconvoluted peaks correspond to SiV center ZPL (1.680 eV) and the double ZPL of the GR1 defect (1.664 eV and the weak shoulder at 1.672 eV).*

Preparation of new tetragonal silicon polymorphs by ultrashort laser pulses. — Tetragonal polymorphs of silicon were created successfully by irradiation of microcrystalline silicon powder with femtosecond laser pulses (800 nm center wavelength with 1 kHz repetition rate and 42 fs pulse duration) in air at room temperature. Surface enhanced Raman spectroscopy and, in collaboration with the Research Institute for Materials Science, Centre for Energy Research, HAS and the Research Centre for Natural Sciences, HAS, transmission electron microscopy (TEM) measurements were carried out to prove the presence of bt8 (Fig. 2) and t32* (Fig. 3) Si phases.

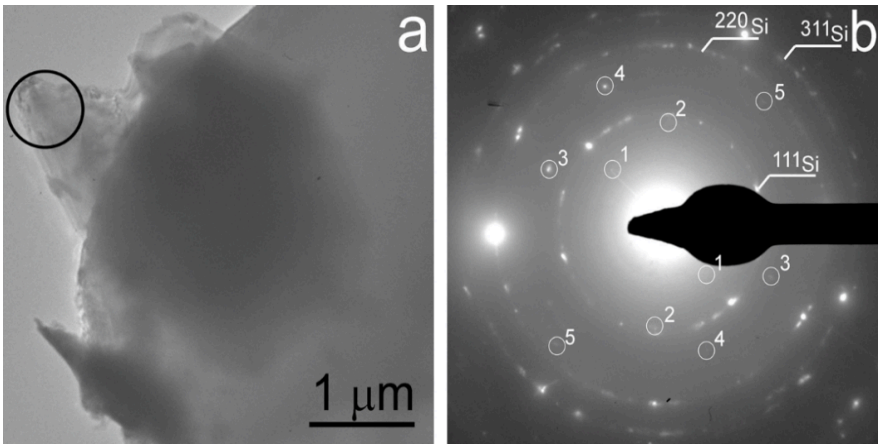

Figure 2. *TEM image of bt8 Si polymorph. In addition to ordinary cubic Si, weak extra reflections occur with the following d spacings: 4.70 (1), 3.37 (2), 2.60 (3), 2.38 (4), 2.10 (5) Å. These extra reflections are consistent with {101} (1), {200} (2), {211} (3), {220} (4) and {301} (5) reflections of bt8 Si.*

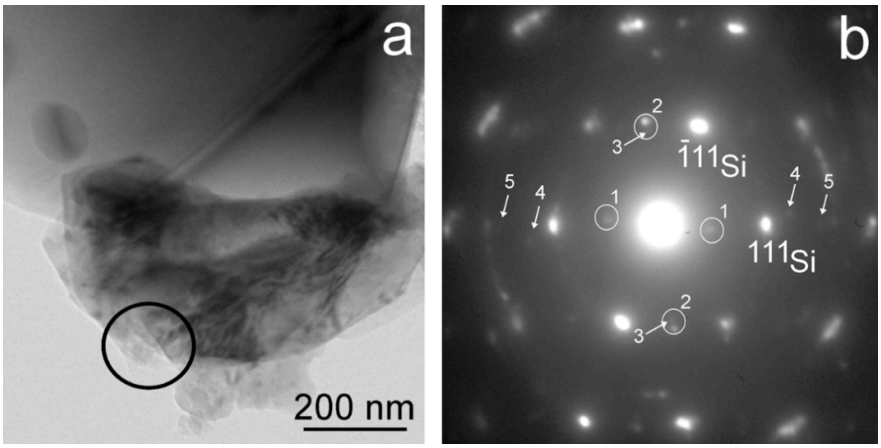

Figure 3. *TEM image of t32* Si polymorph. In addition to ordinary cubic Si, there are two sets of strong reflections with 6.60 (1) and 3.20 (2) Å. These strong reflections and their measured angles are consistent with {110} and {0-12} of t32* Si grain. The additional weak reflections with 3.63 (3), 2.65 (4), 2.16 (5) Å can be interpreted with {211}, {311} and {013} of t32* Si.*